

Design of a Hybrid Airship

Yeo Rui Jovan

NUS High School Of Mathematics And Science

Abstract:

This project explores the possibility of a hybrid airship that generates lift through its wing-like design which is less dependent on hydrostatic buoyancy. Compared to drones or other hybrid airship proposals that rely on use of rotors to generate lift, the design explored here can be optimized for higher speed, yet still retain Short Take-Off and Landing (STOL) characteristics. Airship development stagnated in the 1930s due to safety concerns, but new materials may lead to a renaissance in their design.

The process of designing the hybrid airship started with the finding the optimal airfoil. XFLR5 was used to select an airfoil based on its Coefficient of lift, Coefficient of Drag, and other characteristics under the expected flight parameters. The chosen airfoil was then tested in a wind tunnel to compare the actual characteristics against the expected characteristics, which showed that the characteristics were indeed favorable.

At the same time, a scale model was constructed from carbon fiber, plywood, string, wire and Monokote to get weight characteristics for scaling purposes. Buoyancy characteristics for pressurized helium were also recorded. From the airfoil chosen, the internal volume was calculated, from which the hydrostatic lift that can be produced was derived

Altogether the model in its current dimensions was not neutrally buoyant. However, it was calculated that if it were scaled up by 4 times, it would not only be neutrally buoyant while unloaded, but be able to out-perform contemporary quadcopter drones developed for the purpose of delivery when fully equipped with comparable avionics.

I. BACKGROUND AND PURPOSE

Airships are lighter-than-air aircraft which gain their lift from a lifting gas that is less dense than the surrounding air. They were common in the first days of powered flight, but their use decreased over time as their capabilities were surpassed by those of heavier-than-air aircraft. They still have certain benefits, such as the ability to stay stationary in the air for long periods of time without the need to refuel. They are silent as well when just hovering, as they use their buoyancy to passively stay in position. This means that they have useful applications in the military as well as in scientific research, such as area surveillance.

Airships, however, are restricted by weight limits, as there is a hard limit on how much

weight they can lift while staying less dense than air. This is what this project seeks to address. A hybrid airship in this case would combine the properties of an airship with the lift generating properties of a fixed-wing aircraft, i.e., they can generate lift to carry a payload while moving, but are still able to lift their own weight through buoyancy [1].

An efficient design for such hybrid aircraft is the blended wing-body design, which allows the whole aircraft to generate lift when moving and still gives reasonable volume inside for lifting gas. This brings higher efficiency, as engine power is not being “wasted” in keeping the craft aloft, which can translate to better endurance [1].

Because the body generates lift, the airship must have a rigid-body, so that the lift forces do not cause the wing-body to bend in flight. The target is for the full-scale airship to float unloaded, and be able to hold at least 30% of its unloaded weight while carrying a payload (comparable to the ratio of the STOL(Short Take-Off and Landing) C-130 Hercules [2]), with an intermediate step discussed directly below.

II. SELECTION OF AIRFOIL

This project is a proof-of-concept that can be scaled up by the aerospace industry to be actually used as a remote-delivery drone [3]. The most important element of the scale model that needs to perform is the wing-fuselage. It needs to have a reasonably large internal volume to maximize the volume to surface area ratio, allowing for more lifting gas, and yet retain aerodynamic efficiency. The airfoil was chosen based on comparisons between simulations on the software XFLR5 [4]. If necessary, the airfoil may be thickened to allow for a greater cross-sectional area by up to 1.5 times without significant penalty to flight characteristics [5].

The airfoil should ideally have as large a cross-sectional area as possible to maximize the internal volume of the wing. Coupled with the lower Reynolds number range expected for the prototype (set at 120000 for a projected chord length of 0.60m with the properties of air at 300K), this meant that of the literature searched, only airfoils in the UIUC Airfoil Coordinates Database were of sufficient thickness and low speed performance [5], [6], [7]. These were chosen from proven airfoils to allow some comparison of data. The airfoils that made the final cut for testing in XFLR5 are listed in table 1.

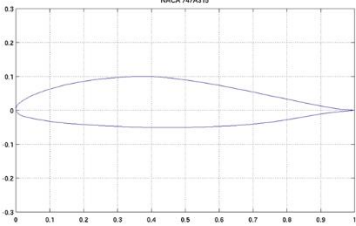
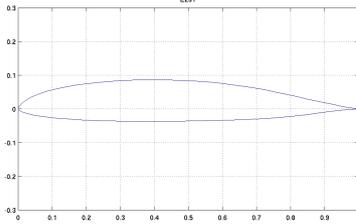
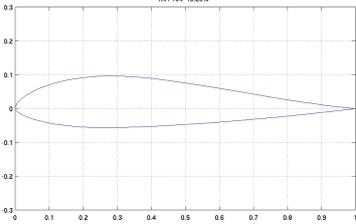
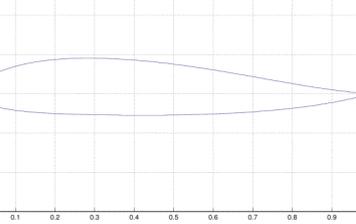
 <p>NACA 747A315</p>	747A315	 <p>E231</p>	Eppler 23
 <p>MH 104 15.28%</p>	MH-104	 <p>GÖE 765 AIRFOIL (recovered)</p>	Göttingen 765 airfoil, abbreviated to ME163 based on its historical use in this paper

Table 1: Profiles of Airfoils used

III. SIMULATION OF PERFORMANCE PARAMETERS

XFLR5 is a software that allows for the calculation of Coefficients of Lift, Drag, Moment, and airflow properties based on user-defined data such as Mach, Reynold's number, and Angle of attack, amongst others. For the purposes of this project, the parameters that were compared were: (i) the C_L against AoA, (ii) C_L against C_D and (iii) C_L/C_D against AoA.

The comparison of selected airfoils was done in an elimination fashion to reduce demands on the software. Below is the reason why one airfoil was chosen over the other, based on the simulation provided by XFLR5, as well as the reason why it was chosen. Reynolds number range was 20000 to 200000, with Mach=0.060 to reflect the likely full-scale parameters. The corresponding XFLR5 data is in Appendix 2.

Trial 1: E231 vs ME163. Both show similar performance in all parameters, but ME163 has the greater cross sectional area of the two, hence E231 was eliminated

Trial 2: 747A315 vs ME163. ME163 shows generally better performance in all three parameters, hence 747A315 was eliminated.

Trial 3: MH-104 vs ME163: Both show similar performance in all parameters, so both were selected for thickening and retesting. Thickening notation for this report is <Name of airfoil>x<Ratio>.

Trial 4: MH-104x1.5 vs ME163x1.5: ME163 retains superior performance in all parameters more effectively when scaling, hence it is chosen over MH-104.

Trial 5: NACA 24xx array compared to ME163 and ME163x1.5: As in Trial 1, both have similar

performance in all parameters, but ME163x 1.5 has a greater cross-sectional area. Hence, ME163x 1.5 was the candidate chosen for wind tunnel trials.

IV. THEORETICAL BASIS OF CALCULATIONS

We assume that lift can be calculated with Bernoulli's Principle, where $\frac{\rho v^2}{2} + \rho g y + P$ is a constant K, and the gravitational term $\rho g y$ is negligible in air for a static pressure force, as well as the dynamic pressure associated with the downward deflection of air produced by the positive AoA. The following can hence be derived: $\frac{\rho(v_{acc}^2 - v^2)}{2} = \frac{L}{S}$, and from which we can obtain an expression for coefficient of lift at 0 degrees AoA: $\frac{2L}{\rho v^2 S} = \frac{v_{acc}^2}{v^2} - 1 = C_L = \frac{2L}{x} \cdot \frac{\rho c}{R^2 \mu^2} = \frac{2L \rho c}{x R^2 \mu^2}$

We therefore expect the lift to increase with the square of the Reynold's Number (A full derivation is available in Appendix 6).

V. EXPERIMENTAL TESTING OF MODEL

Once the airfoil was chosen, the surface area and volume of the model was calculated. To simplify construction, no wing tapering or sweep was used. Wind tunnel tests of the selected design were performed to confirm the data, using two kinds of models: one to test mass predictions and one to test aerodynamic performance.

The wind tunnel is a refurbished wind tunnel left behind from an unrelated student's project. It was modified to include a weighing scale with an accuracy of 0.1g and an anemometer with an accuracy of 0.1m/s. It has 3 speed settings, which are 2.2m/s, 2.5-2.6m/s, and 2.9-3m/s

For mass predictions, the model's weight was recorded throughout the construction process. Calibration of the lifting potential of helium also occurred. It consists of two wooden chord panels on either end to provide the shape of the airfoil which are held together by 4 carbon fiber rods to

provide rigidity. To maintain the shape of the airfoil, metal wire is laid at strategic points longitudinally and cotton thread is laid transversally. The inside was hollow so that gas sacs. Each plywood panel has its center cut out to leave a 2cm thick inner margin.

VI. AERODYNAMIC TESTING AND RESULTS

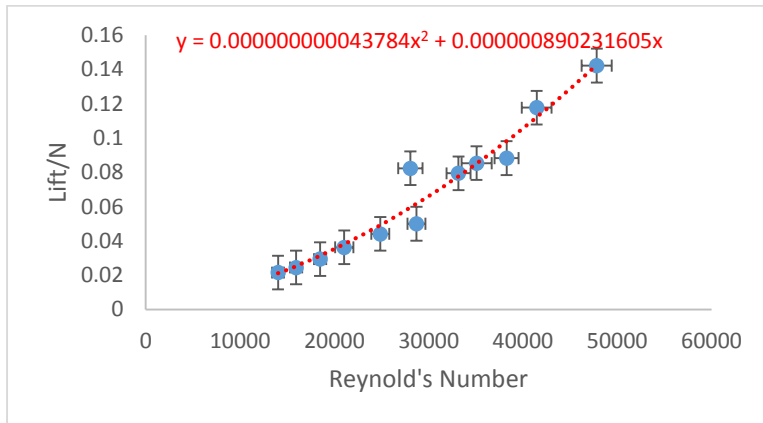


Figure 1 Graph of Lift against Reynold's Number

3D-printed airfoil sections of ME163x1.5 were made for wind tunnel usage. Their dimensions are listed in Appendix 4. The following table plotted from Table 4.3 in Appendix 4 shows the power relation between

Reynold's Number and Lift force. This graph shows a close fit to the predicted trendline of Equation 1.

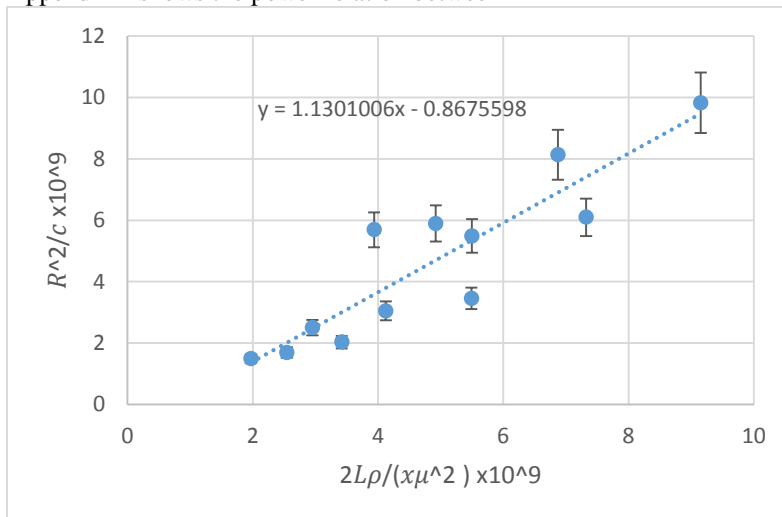


Figure 2 Linearised graph

This graph plotted shows the roughly linear relation between $\frac{R^2}{c}$ and $\frac{2L\rho}{x\mu^2}$. The gradient is the Coefficient of lift at 0 degrees Angle of attack. We see $C_L=1.13$, and the linear regression calculations from Table 4.4 give an r^2 value of 0.8164.

VIII. MASS TESTING AND RESULTS

VII. CAVEAT

When we compared the extreme low lift range of $C_L = 0.4-0.8$, we found that the lift was anomalously high. We have insufficient data to analyze this, but we suspect wingtip vortices are involved. For the rest of the paper, we shall treat the C_L to be 0.56, or half the value of 1.13 found earlier.

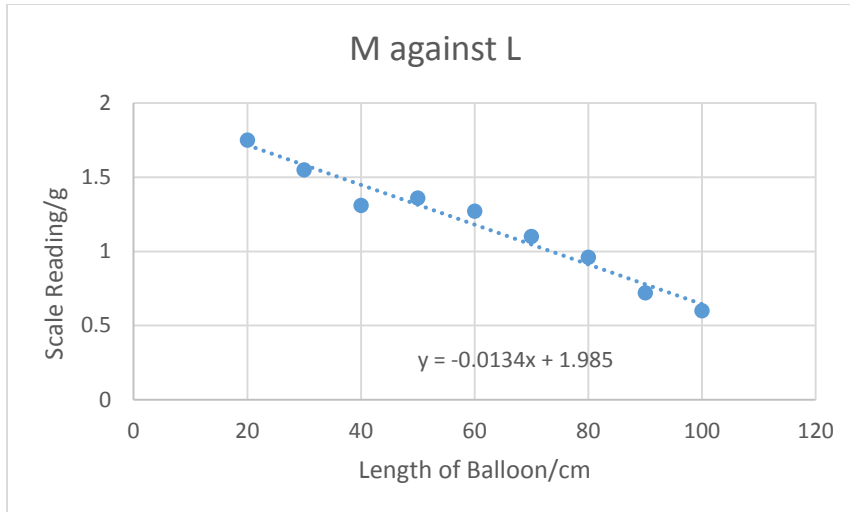


Figure 3 Mass of balloon against Length

Next we consider the hydrostatic lift of the airship. The buoyancy of helium under expected pressure was tested. The balloons were inflated to different lengths, and the data was recorded. The gradient of the resulting graph is -0.0134g/cm , which is the extra liftable mass in grams per centimeter length of balloon. Considering the inflated diameter of the balloon to be 14cm , the liftable mass of pressurized helium is 858.97g/m^3

Using the density of air and the density of Helium [9] we have the expected liftable mass to be 1014.57g/m^3 , hence showing that pressurization should account for roughly 15.33% loss in liftable mass. The Cross-Sectional area of the airfoil is 0.0512m^2 , as found through integration, hence the internal volume of the model, assuming all components have negligible thickness is 0.0614m^3 . The helium contained would be able to lift 52.7g , or 22.1% of its current mass. From scaling considerations (see Appendix 6), we can calculate the final lift to mass ratio is given by the following equations:

$$m_{sys} = 0.0614 \cdot 858.97 \cdot a \cdot b^2 - 56.07a - 73.68b - 153.75ab$$

$$\frac{\sum \text{Liftablemass}_{scaled} - \sum \text{Mass}_{scaled}}{\sum \text{Mass}_{scaled}}$$

$$= \frac{m_{sys}}{\sum \text{Mass}_{scaled}}$$

$$= \frac{0.0614 \cdot 858.97 \cdot a \cdot b^2 - 56.07a - 73.68b - 153.75ab}{56.07a + 73.68b + 153.75ab}$$

For the case where $a=b$, the scaling factor of the airship for it to be neutrally buoyant is $a=b=3.6$

IX. SCALINGS

We shall round up the above value of 3.6 to 4, to factor in the extra materials needed for strengthening needed due to scale. At the same time, the materials used can be optimized, with Mylar used for the covering instead of Monokote. The Monokote was quoted as 61.03g/m^2 [10], and 0.03mm thick Mylar is 41.70g/m^2 [11], assuming that aluminizing the Mylar adds a negligible

amount of weight. At these dimensions, the airship would weigh 2979g and be able to lift through hydrostatic lift only 3375g .

To carry an extra 2.8kg of payload (50% of its mass factoring in the flight systems, which includes power sources, GPS, motors, and control surfaces are expected to weigh up to 2kg) at a velocity of 3.57m/s or 12.81km/h for a total of 4.8kg , the Reynold's number has to be at least 480000 , giving a drone with a footprint of $2.4 \times 4.8\text{m}$. This compares favorably with the current drone system that DHL is experimenting with which has a footprint of $1.1\text{m} \times 1.1\text{m}$ and a lift capability of 1.2kg [12]. Data on Amazon's Octocopter is scarce at the time of writing, but its payload is projected at double that of the DHL drone and its footprint is unknown. For cruising at the proposed speed of 20km/h , the Reynold's number would be about 1000000 , the airship could lift 16.9kg , which is superior to both known competitors. However, in order to lift these payloads, hover and VTOL are not viable.

X. STOL CAPABILITIES

Assuming similar avionics and engines to the DHL drone, the maximal thrust that can be produced is 118N [12], which when loaded with the stated 4.8kg load and assuming that drag is negligible, to reach a speed of 20km/h during take-off would take 1.5s . Factoring in drag and other factors, the minimal take-off and landing distance would be about 10m of rough-field conditions if reverse thrust is available

XI. PROPOSED USE OF FULL SCALE DESIGN

The above problem brings us back to the proposed use of the hybrid airship as a more efficient alternative to the DHL drone. Due to the size difference and the inability to hover whilst carrying payload, over shorter distances, the current drone is superior. But over longer distances, the lack of VTOL (Vertical Take-Off and Landing)

of the hybrid airship will be an acceptable trade-off for increased range and speed, which would be useful for conditions such as supplying first-aid responders with extra supplies in emergency

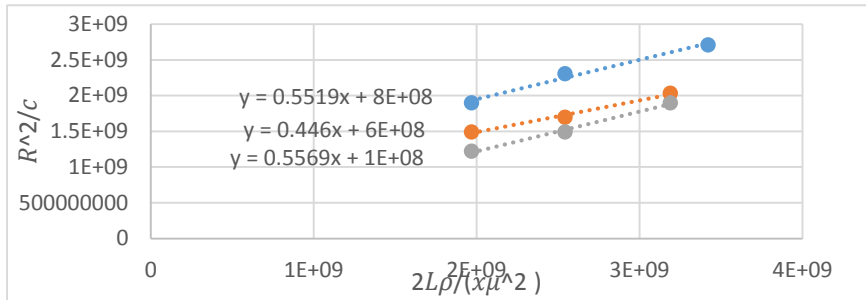
situations. In fact, when given a landing platform, the airship will be more useful than the DHL drone when it comes to its original purpose of medication delivery [3].

REFERENCES

- All airfoils are from http://m-selig.ae.illinois.edu/ads/coord_database.html, or generated by XFLR5. Air properties from http://www.engineeringtoolbox.com/dry-air-properties-d_973.html
- [1]: Barocela, E., & Cassidy, P. F. (2006). *U.S. Patent No. 7,137,592*. Washington, DC: U.S. Patent and Trademark Office.
- [2]: US: Air Force, (2003, September 1). *C-130 Hercules*. Retrieved from <http://www.af.mil/AboutUs/FactSheets/Display/tabid/224/Article/104517/c-130-hercules.aspx>
- [3]: DHL Press Release, (2014, September 24). *DHL Parcelcopter launches initial operations for research purposes*. Retrieved from http://www.dhl.com/en/press/releases/releases_2014/group/dhl_parcelcopter_launches_initial_operations_for_research_purposes.html
- [4]: Deperrois, A. (2010). *XFLR5: a tool for the design of airfoils, wings and planes operating at low Reynolds numbers*. Software Package.
- [5]: Selig, M. S. (Ed.). (1995). *Summary of low speed airfoil data* (Vol. 1). SoarTech.
- [6]: Jacobs, E. N. (1932). *The aerodynamic characteristics of eight very thick airfoils from tests in the variable density wind tunnel*. National Advisory Committee for Aeronautics.
- [7]: UIUC Applied Aerodynamics Group (2013, January 25). UIUC Airfoil Coordinates Database, Retrieved from http://m-selig.ae.illinois.edu/ads/coord_database.html
- [8]: Selig, M. S. (Ed.). (1997). *Summary of low speed airfoil data* (Vol. 3). SoarTech.
- [9]: Air Products (1994, March). *Materials Safety Data Sheet-Helium*. Retrieved from <http://avogadro.chem.iastate.edu/MSDS/helium.pdf>
- [10]: Top Flite (1999). *Econokote*. Retrieved from <http://downloads.hobbico.com/sellsheets/top/topq2601-sell-sheet.pdf>
- [11]: The Gund Company. *Material Data Sheet*. Retrieved from <http://thegundcompany.com/files/index.cfm?pdfpath=Mylar%20EL%20MO%20Polyester%20Film1.pdf>
- [12]: Microdrones (2014, June 23). md4-1000. Retrieved from <http://wiki.microdrones.com/index.php/md4-1000>

Appendix 1: Note on the Adjusted C_L Value

Dimension	V	Reynolds Number	Lift/N	Span/M	X-axis R^2/C	Multiplier p/u^2	C_L	Y-axis
0.1	2.2	14030.61224	0.013734	0.05	1968580800	6907852650	0.963866439	1897448966
0.1	2.5	15943.87755	0.016677	0.05	2542072314	6907852650	0.906364921	2304045173
0.1	2.9	18494.89796	0.01962	0.05	3420612505	6907852650	0.792443276	2710641380
0.1	2.2	14030.61224	0.021582	0.1	1968580800	6907852650	0.757323631	1490852759
0.1	2.5	15943.87755	0.024525	0.1	2542072314	6907852650	0.666444795	1694150862
0.1	2.8	17857.14286	0.02943	0.1	3188775510	6907852650	0.637542853	2032981035
0.1	2.2	14030.61224	0.026487	0.15	1968580800	6907852650	0.619628425	1219788621
0.1	2.5	15943.87755	0.032373	0.15	2542072314	6907852650	0.58647142	1490852759
0.1	2.8	17857.14286	0.041202	0.15	3188775510	6907852650	0.595039996	1897448966



ignored span-wise effects. The cause of the airfoils tested having an inflated C_L value is beyond the scope of this project and the capabilities of the apparatus used.

From the derivation of C_L we can see that the following can be derived:

$$C_L = \frac{2\Delta p}{\rho v^2}$$

Hence the pressure difference per unit wing is constant, leading to similar C_L values as seen from the similar gradients as seen from the graph.

However the individual data points show a different phenomenon at play, with the total C_L decreasing asymptotically with span, approaching the expected values as given by XFLR5. XFLR5 assumed an infinitely long airfoil and

Appendix 2: Airfoil Cross-Sections for Visual Reference

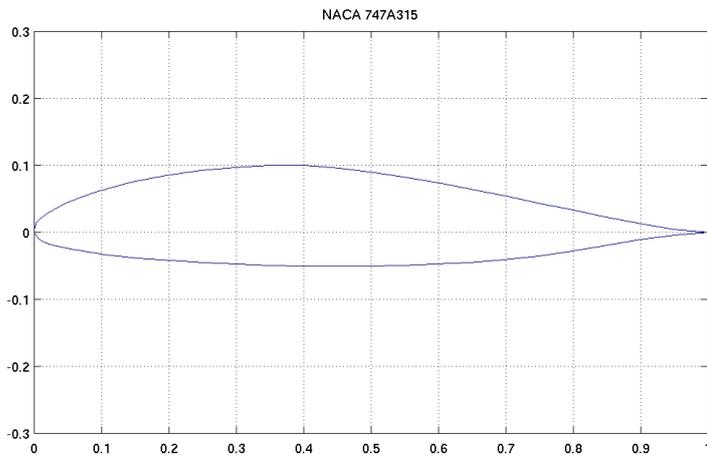


Figure 2.1: 747A315 Airfoil, rejected, image from <http://m-selig.ae.illinois.edu/ads/afplots/naca747a315.gif>

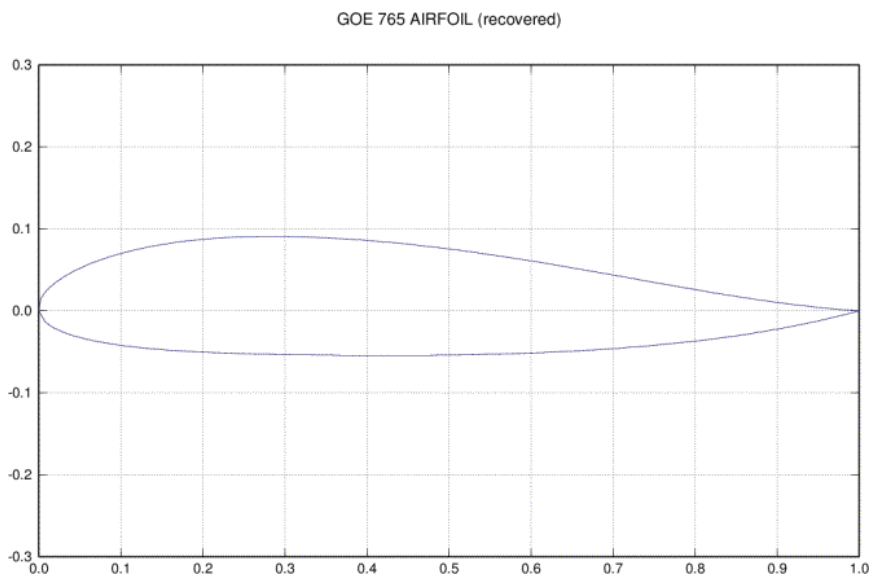


Figure 2.2: ME163 Airfoil, Selected to be thickened to 1.5 times original thickness, image from <http://robdebie.home.xs4all.nl/me163/images/go765-062.gif>

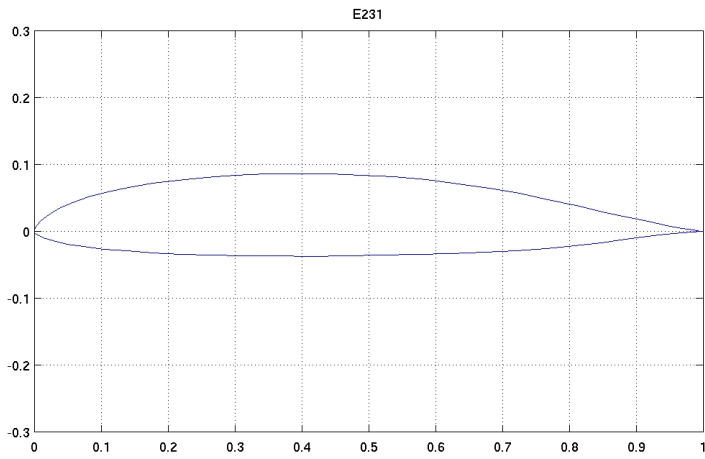


Figure 2.3: E231 Airfoil, rejected, image from <http://m-selig.ae.illinois.edu/ads/afplots/e231.gif>

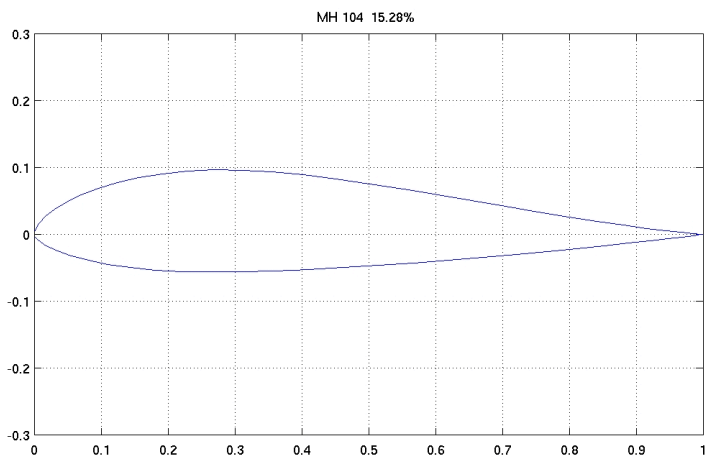


Figure 2.4, MH-104 Airfoil, rejected, image from <http://m-selig.ae.illinois.edu/ads/afplots/mh104.gif>

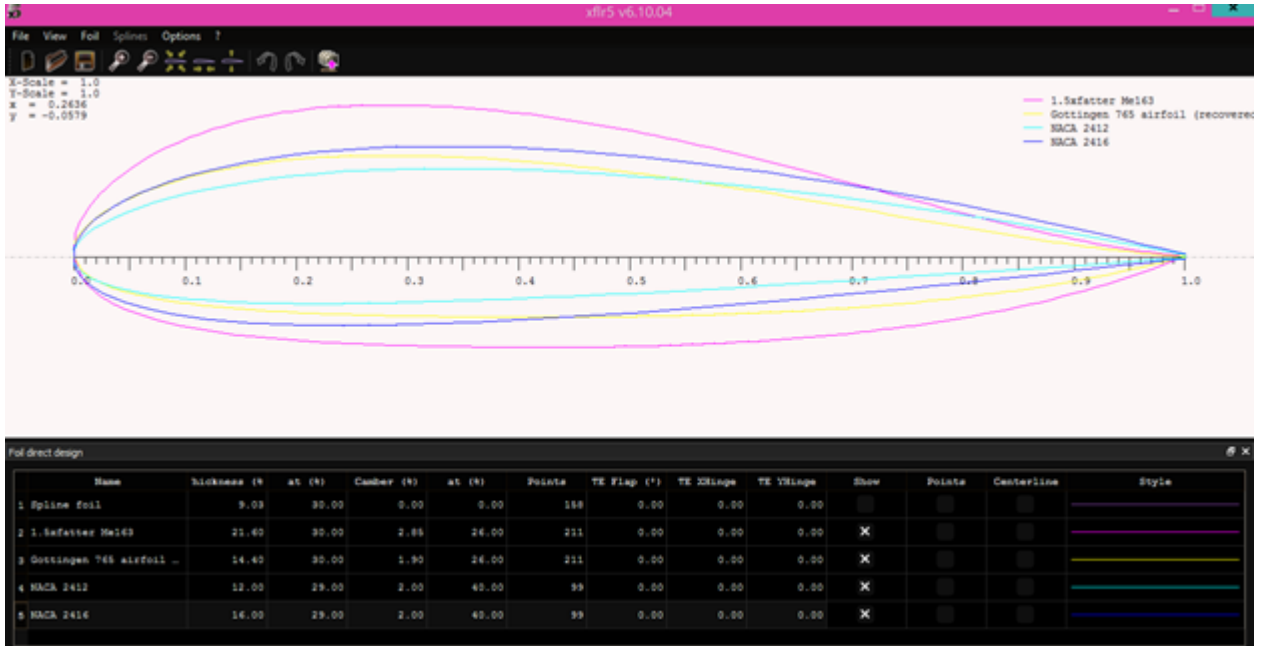


Figure 2.5, NACA 24xx array compared to ME163 Airfoil and ME163x1.5 Airfoil, image self-generated

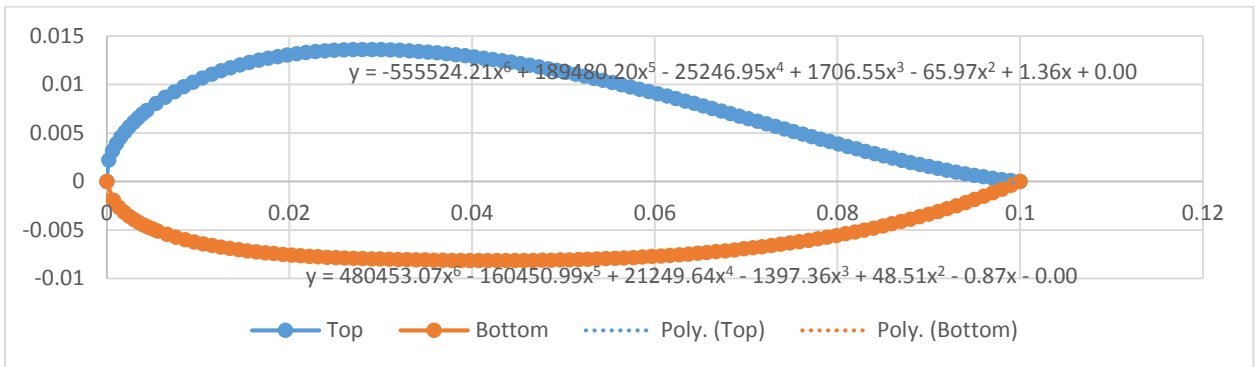


Figure 2.6: ME163x1.5 Airfoil, overall selected, image self-generated. Equations for the upper and lower surface are included for calculation of the cross-sectional area

Appendix 3: XFLR5 Data

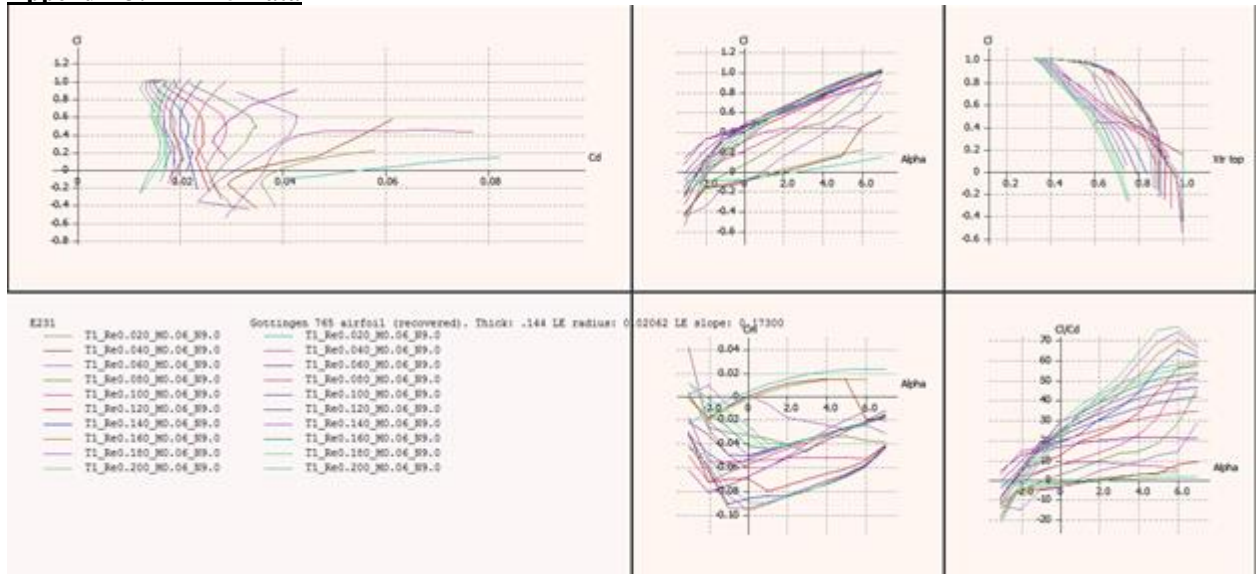


Figure 3.1: Trial 1: E231 vs ME163

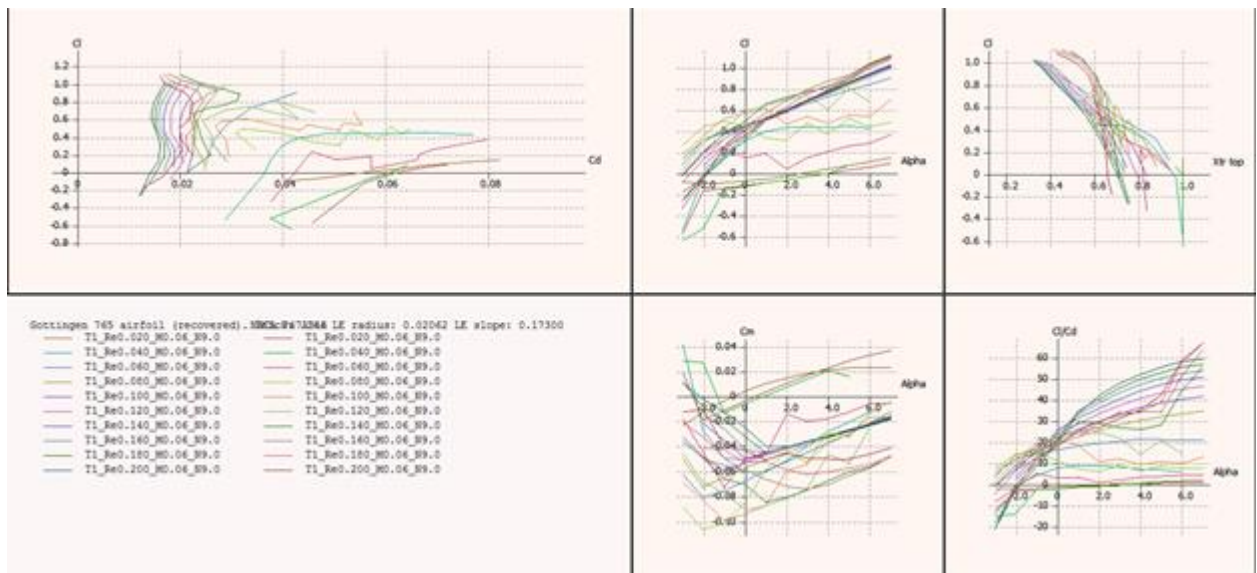


Figure 3.2: Trial 2: 747A315 vs ME163

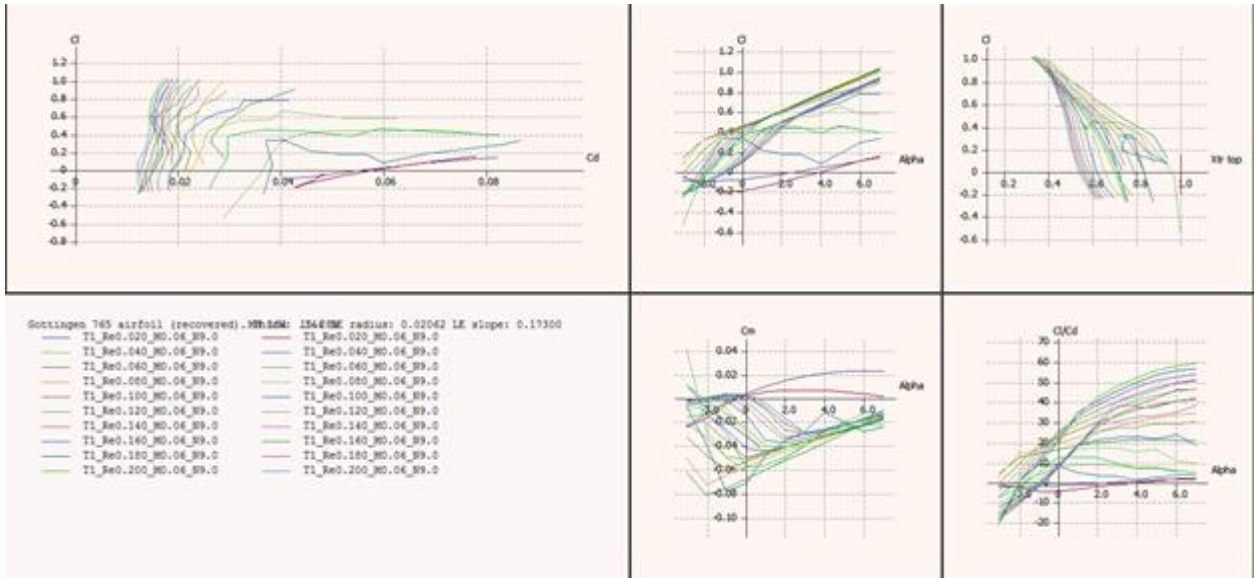


Figure 3.3: Trial 3: MH-104 vs ME163

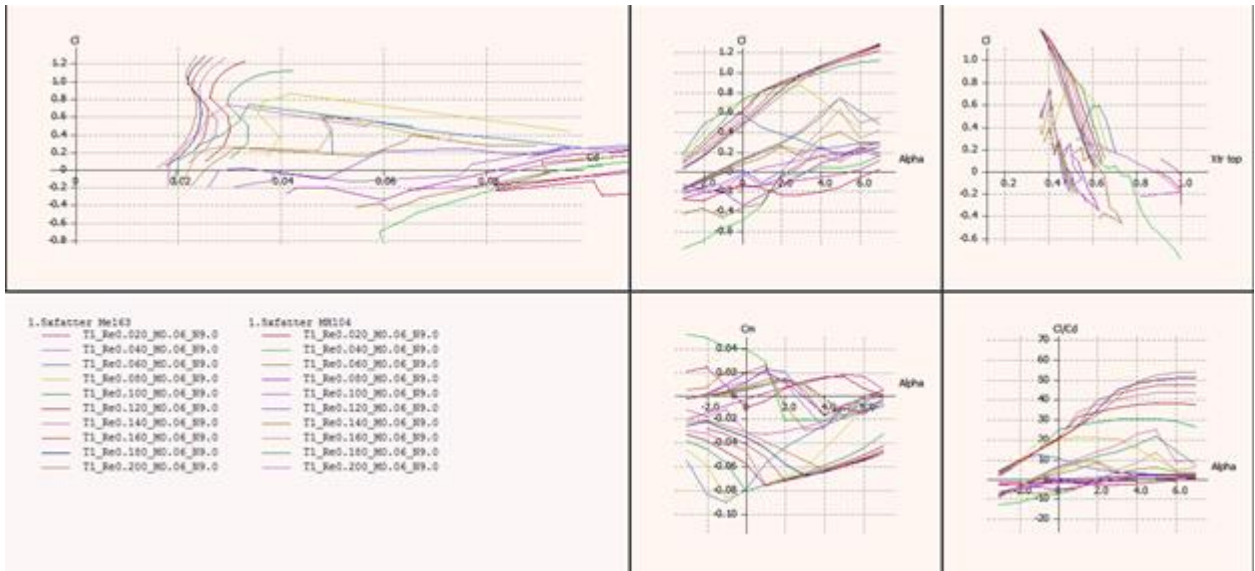


Figure 3.4: Trial 4: MH-104x1.5 vs ME163x1.5

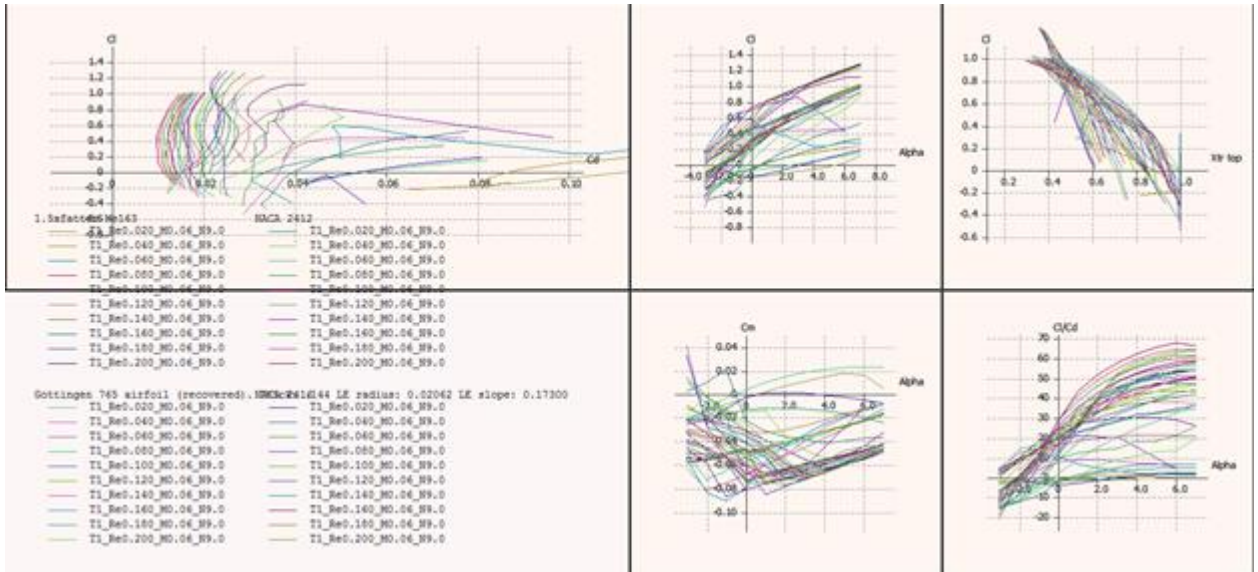


Figure 3.5: Trial 5: NACA 24xx array compared to ME163 Airfoil and ME163x1.5 Airfoil

Appendix 4: Wind Tunnel Data

Chord/cm	Span/cm
10	5
10	10
10	15
15	10
20	10
25	10

Table 4.1: Dimensions of 3D-printed airfoils, all using ME163x1.5 as base



Figure 4.2: Wind Tunnel Set-up

Dimension	V	Kinematic Viscosity of air, 300K	Reynolds Number	Lift/g	Lift/N	X Error	Y Error
0.1	2.2	0.00001568	14030.61224	2.2	0.021582	637.755102	0.00981
0.1	2.5	0.00001568	15943.87755	2.5	0.024525	637.755102	0.00981
0.1	2.9	0.00001568	18494.89796	3	0.02943	637.755102	0.00981
0.15	2.2	0.00001568	21045.91837	3.7	0.036297	956.6326531	0.00981
0.15	2.6	0.00001568	24872.44898	4.5	0.044145	956.6326531	0.00981
0.15	3	0.00001568	28698.97959	5.1	0.050031	956.6326531	0.00981
0.2	2.2	0.00001568	28061.22449	8.4	0.082404	1275.510204	0.00981
0.2	2.6	0.00001568	33163.26531	8.1	0.079461	1275.510204	0.00981
0.2	3	0.00001568	38265.30612	9	0.08829	1275.510204	0.00981
0.25	2.2	0.00001568	35076.53061	8.7	0.085347	1594.387755	0.00981
0.25	2.6	0.00001568	41454.08163	12	0.11772	1594.387755	0.00981
0.25	3	0.00001568	47831.63265	14.5	0.142245	1594.387755	0.00981

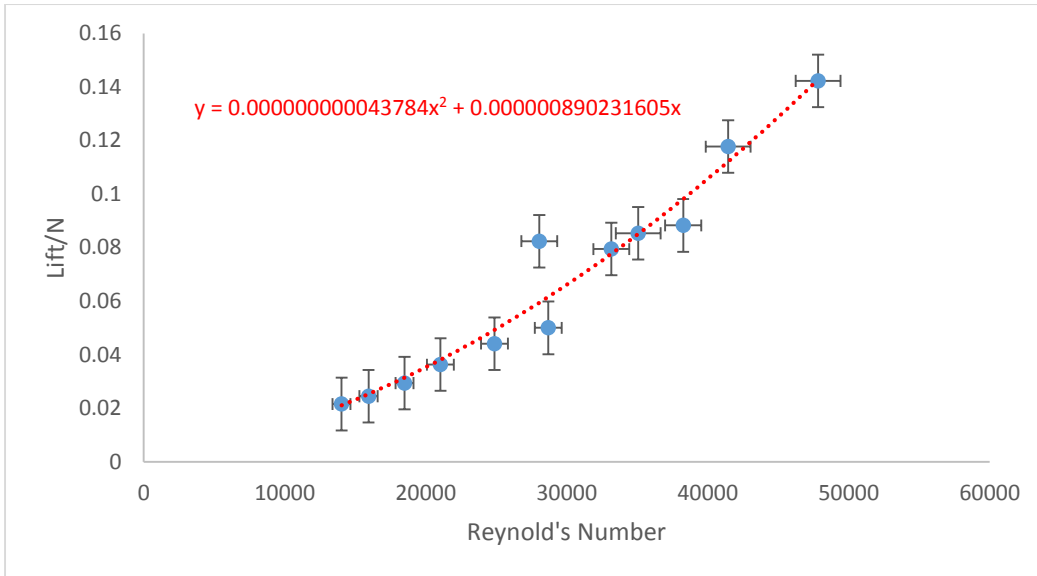


Table 4.3: Data collected for the sections of 10cm Span at 0 degrees Angle of attack and associated graph

Chord/m	V/m/s	Reynolds Number	Lift/g	Lift/N	R ² /C (X-Axis)	L/x	Multiplier p/u ²	CL	Y-Axis
0.1	2.2	14030.61224	2.2	0.021582	1968580800	0.21582	6907852650	0.757323631	1490852759
0.1	2.5	15943.87755	2.5	0.024525	2542072314	0.24525	6907852650	0.666444795	1694150862
0.1	2.9	18494.89796	3	0.02943	3420612505	0.2943	6907852650	0.594332457	2032981035
0.15	2.2	21045.91837	3.7	0.036297	2952871200	0.36297	6907852650	0.849120435	2507343276
0.15	2.6	24872.44898	4.5	0.044145	4124258122	0.44145	6907852650	0.739398811	3049471552
0.15	3	28698.97959	5.1	0.050031	5490876197	0.50031	6907852650	0.629420084	3456067759
0.2	2.2	28061.22449	8.4	0.082404	3937161599	0.82404	6907852650	1.445799659	5692346897
0.2	2.6	33163.26531	8.1	0.079461	5499010829	0.79461	6907852650	0.998188395	5489048794
0.2	3	38265.30612	9	0.08829	7321168263	0.8829	6907852650	0.833055994	6098943104
0.25	2.2	35076.53061	8.7	0.085347	4921451999	0.85347	6907852650	1.197948289	5895645001
0.25	2.6	41454.08163	12	0.11772	6873763536	1.1772	6907852650	1.183038098	8131924139
0.25	3	47831.63265	14.5	0.142245	9151460329	1.42245	6907852650	1.073716614	9826075002

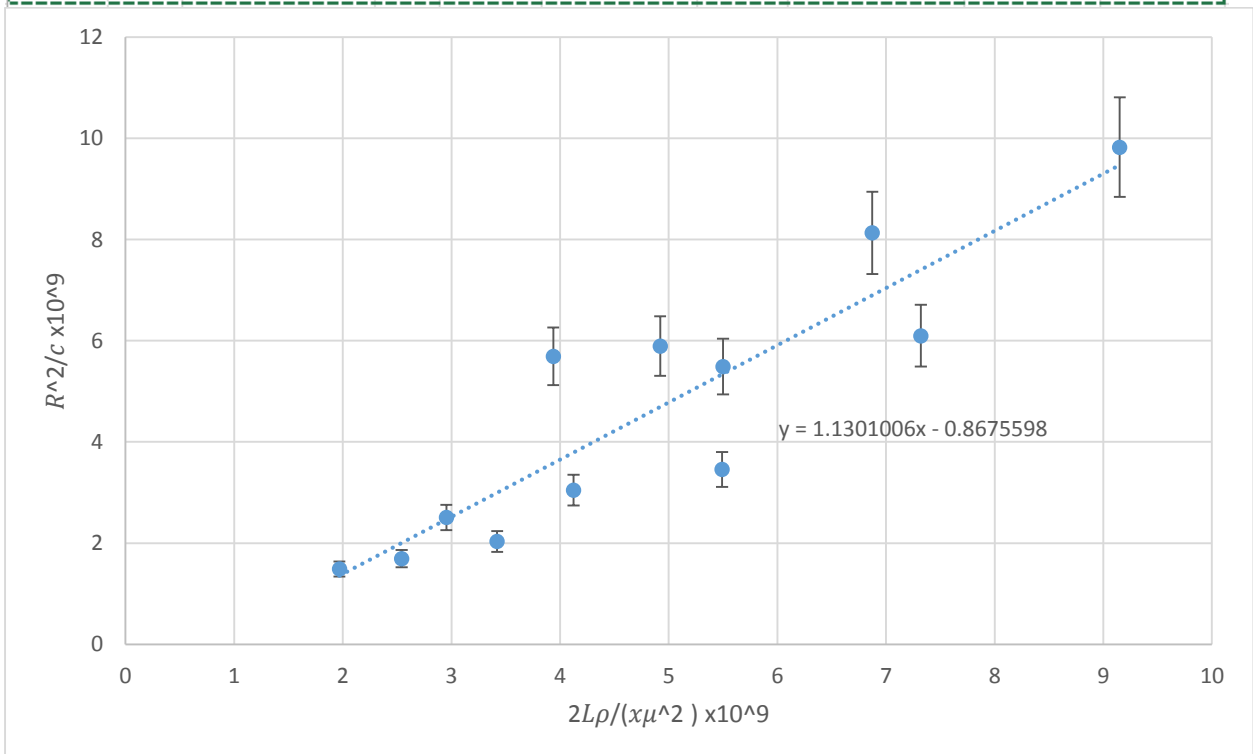


Table 4.4: Data collected for the sections of 10cm Span at 0 degrees AoA, factoring in Equation 1 and associated graph

Kinematic Viscosity of air, 300K	0.00001568 m ² /s
Dynamic Viscosity of air, 300K	0.00001846 kg/ms
Density of Air, 3000K	1.177 kg/m ³

Table 4.5: Data of the properties of air used, retrieved from http://www.engineeringtoolbox.com/dry-air-properties-d_973.html

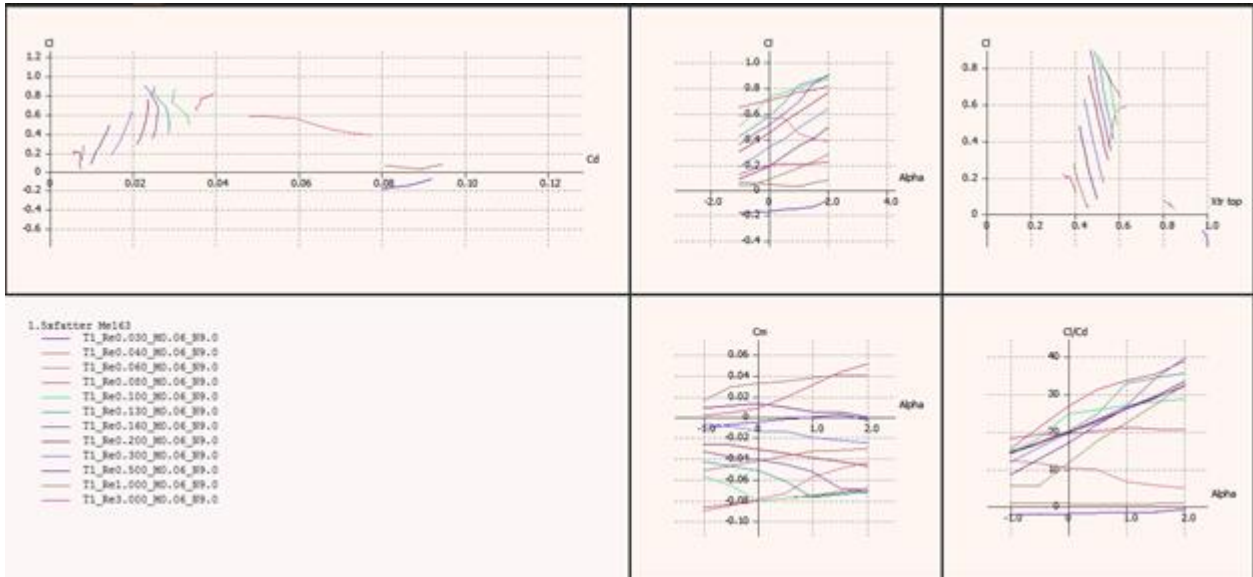


Figure 4.6: Ideal data for ME163x1.5 at Reynolds number range from 30000 to 3000000, with Mach=0.060, AoA range is limited to -1 to +2 Degrees to serve as a comparison to the wind tunnel data. It is interesting to note that below Reynolds Number=800000, flow behaves differently as seen from the C_L/C_D data

Appendix 5: Mass and Helium Data

Part	Quantity	Mass/g	Mass per unit	Units
4x1.2m Carbon fibre rods	1.2	56.07	46.725	g/m
Plywood endplates, 2cm margin	2	73.68	36.84	g
Monokote, Strings, Wire Covering	1.44	153.75	106.7708333	g/m ²
Total		283.5		

Table 5.1: Mass breakdown of component parts

Length/cm	Mass/g
20	1.75
30	1.55
40	1.31
50	1.36
60	1.27
70	1.1
80	0.96
90	0.72
100	0.6

Balloons used were sculpting balloons. Each balloon has an empty mass of 2.01g. When inflated, it has a diameter of 14cm and a cross sectional area of 15.60 cm².

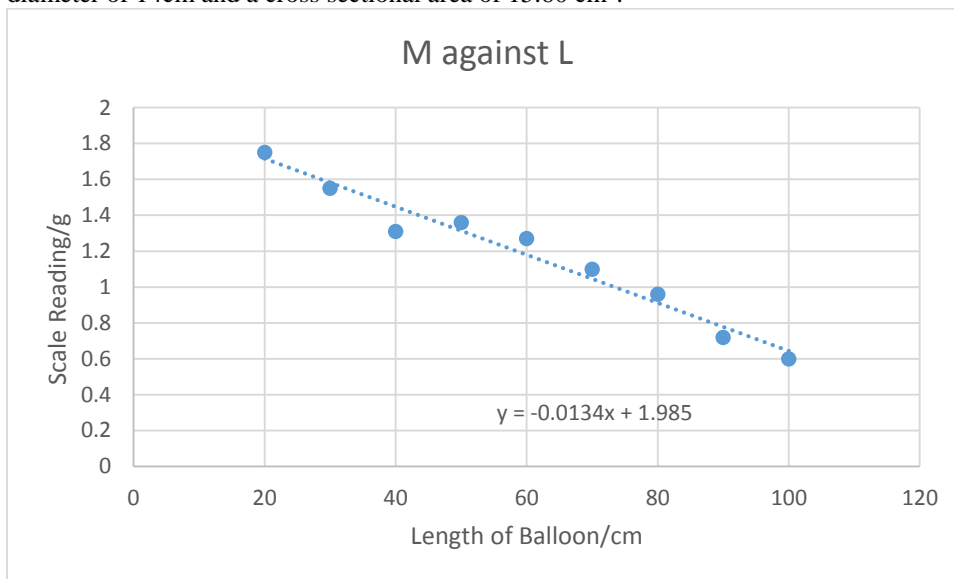


Table 5.2: Lifting properties of pressurized Helium and associated graph

Part	Dimensions	Notes
Plywood	3mm thick, section 58.5cm long	Center cut out
Carbon fibre	4mm diameter, 2.5mm inner diameter, 1.2m long	Hollow
Balloon	30cm long, 0.28mm thick	Uninflated

Table 5.3: Notes on materials used in construction of the model

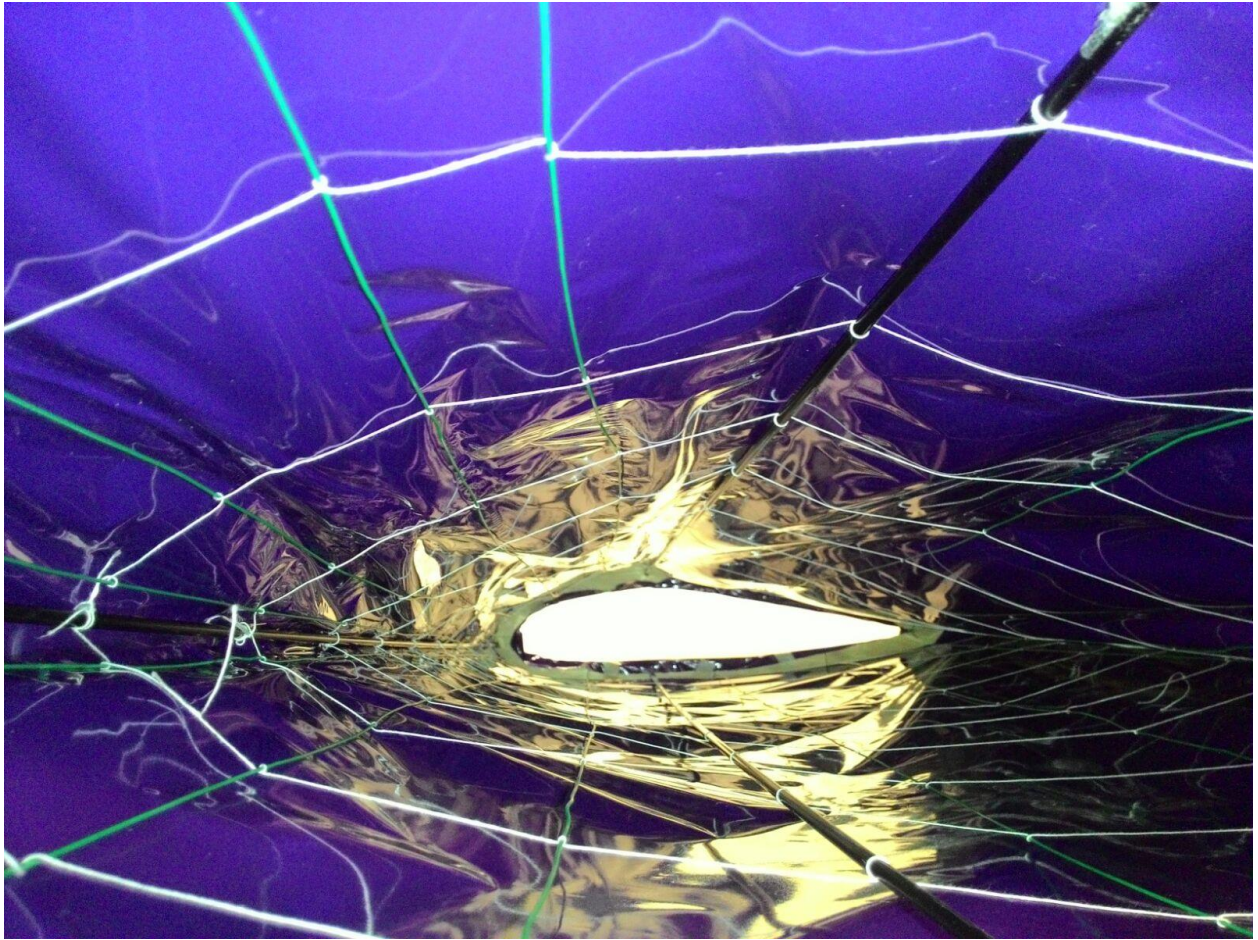


Figure 5.4: View of the inside of the model. 3 carbon fibre rods can be seen, as well as the longitudinal wires and the transverse cotton threads.

Chord x4, Span x4						
Part	Mass/unit	Units	Scale	Coefficient	Mass/g	
4x1.2m Carbon fibre rods	56.07	g	Linear	4	224.28	
2 Plywood endplates, 2cm margin	73.68	g	Linear	4	294.72	
Monokote, Strings, Wire Covering	153.75	g/m ²	Dependent	16	2460	
Total					2979	
	Value	Units			Value	Units
Cross-sectional area	0.0512	m ²	Square	16	0.8192	m ²
Volume	0.0614	m ³	Dependent	64	3.9296	m ³
Lift	858.97	g/m ³	Constant	1	3375.408512	g
Buoyant, Mass < Lifiable Mass	2979	<	3375.40851			
Net	396.408512					

Table 5.5: Table of mass calculations if the chord and the span scale by 4 times

Appendix 6: Derivations

Let:

AoA=Angle of Attack

R=Reynold's Number

C_L =Coefficient of lift

ρ =Density

μ =Dynamic viscosity

ν =Kinematic viscosity

v =True Velocity

v_{acc} =Velocity of accelerated air

S =Plan area

x =Span

c =Chord

L =Lift force

K =Constant

P =Pressure

g =Gravitational acceleration

y =Change in height

m =Mass

a =Scale in span with reference to the original model

b =Scale in chord with reference to the original model

A =Cross-Sectional Area

Bernoulli's Principle:

$$\frac{\rho v^2}{2} + \rho g y + P = K$$

Since gravitational term $\rho g y$ is negligible in air for a static pressure force, as well as a dynamic pressure associated with the downward deflection of air produced by the positive AoA:

$$\frac{\rho v_{acc}^2}{2} + P_{upper} = \frac{\rho v^2}{2} + P_{Lower}$$

Since air on the upper surface is accelerated, $P_{upper} < P_{Lower}$

$$\frac{\rho v_{acc}^2}{2} - \frac{\rho v^2}{2} = P_{Lower} - P_{upper} = \Delta P, \Delta P = \frac{L}{S}$$

$$\frac{\rho(v_{acc}^2 - v^2)}{2} = \frac{L}{S}$$

$$\frac{\rho(\frac{v_{acc}^2}{v^2} - 1)v^2 S}{2L} = 1, \therefore \frac{2L}{\rho(\frac{v_{acc}^2}{v^2} - 1)v^2 S} = 1$$

$$\frac{2L}{\rho v^2 S} = \frac{v_{acc}^2}{v^2} - 1 = C_L$$

We now have the coefficient of lift, which is useful for plotting graphs

$$C_L = \frac{2L}{\rho v^2 S}, S = cx, \therefore C_L = \frac{2L}{\rho v^2 cx}$$

$$C_L = \frac{2L}{x} \cdot \frac{\rho c}{(\rho v c)^2}, R = \frac{\rho v c}{\mu}, \therefore C_L = \frac{2L}{x} \cdot \frac{\rho c}{(\rho v c)^2} \cdot \frac{\mu^2}{\mu^2}$$

$$C_L = \frac{2L}{x} \cdot \frac{\rho c}{R^2 \mu^2} = \frac{2L \rho c}{x R^2 \mu^2}$$

To Summarize:

$$\frac{2L}{\rho v^2 S} = \frac{v_{acc}^2}{v^2} - 1 = C_L = \frac{2L}{x} \cdot \frac{\rho c}{R^2 \mu^2} = \frac{2L \rho c}{x R^2 \mu^2} \dots \text{Equation 1}$$

X-axis: $\frac{R^2}{c}$

Y-axis: $\frac{2L \rho}{x \mu^2}$

Y/X will hence be C_L for Table 4.4

For the scaling equations:

$$\sum \text{Mass} = m_{carbonfibre} + m_{wood} + m_{skin}$$

Factoring in scale factors a and b and the known masses of each component from Appendix 5:

$$\sum Mass_{scaled} = 56.07a + 73.68b + 153.75ab$$

Since the liftable mass of pressurized helium is found to be 858.97g/m³ and its volume is 0.0614m³, we have the expression of the scaling of the liftable mass:

$$\sum Liftablemass_{scaled} = 0.0614 \cdot 858.97 \cdot a \cdot b^2$$

Hence the extra mass in flight systems and payload is determined as such:

$$m_{sys} = \sum Liftablemass_{scaled} - \sum Mass_{scaled}$$

$$m_{sys} = 0.0614 \cdot 858.97 \cdot a \cdot b^2 - 56.07a - 73.68b - 153.75ab \dots \text{Equation 2}$$

For the case where a=b, the scaling factor of the airship for it to be neutrally buoyant is a=b=3.6

The lift to mass ratio through hydrostatic lift only is given to be:

$$\frac{\sum Liftablemass_{scaled} - \sum Mass_{scaled}}{\sum Mass_{scaled}} = \frac{m_{sys}}{\sum Mass_{scaled}}$$

$$= \frac{0.0614 \cdot 858.97 \cdot a \cdot b^2 - 56.07a - 73.68b - 153.75ab}{56.07a + 73.68b + 153.75ab} \dots \text{Equation 3}$$